High-precision measurements of the co-polar correlation coefficient: non-Gaussian errors and retrieval of the dispersion parameter μ in rainfall

Article

Accepted Version

It is advisable to refer to the publisher's version if you intend to cite from the work. See Guidance on citing.

To link to this article DOI: http://dx.doi.org/10.1175/JAMC-D-15-0272.1

Publisher: American Meteorological Society

the End User Agreement.

www.reading.ac.uk/centaur

CentAUR

Central Archive at the University of Reading

Reading's research outputs online

High-Precision Measurements of the Co-Polar Correlation

Coefficient: Non-Gaussian Errors and Retrieval of the Dispersion

Parameter μ in Rainfall

W. J. KEAT, * C. D. WESTBROOK, AND A. J. ILLINGWORTH

Department of Meteorology, University of Reading, UK

_____

* *Corresponding author address:* W. J. Keat, Department of Meteorology, University of Reading, Earley Gate, PO Box 243, Reading, RG6 6BB.

E-mail: w.j.keat@pgr.reading.ac.uk

ABSTRACT

The co-polar correlation coefficient (ρ_{hv}) has many applications, including hydrometeor classification, ground clutter and melting layer identification, interpretation of ice microphysics and the retrieval of rain drop size distributions (DSDs). However, we currently lack the quantitative error estimates that are necessary if these applications are to be fully exploited. Previous error estimates of ρ_{hv} rely on knowledge of the unknown 'true' ρ_{hv} and implicitly assume a Gaussian probability distribution function of ρ_{hv} samples. We show that frequency distributions of ρ_{hv} estimates are in fact highly negatively skewed. A new variable: $L = -\log_{10}(1 - \rho_{hv})$ is defined, which does have Gaussian error statistics, and a standard deviation depending only on the number of independent radar pulses. This is verified using observations of spherical drizzle drops, allowing, for the first time, the construction of rigorous confidence intervals in estimates of ρ_{hv}. In addition, we demonstrate how the imperfect co-location of the horizontal and vertical polarisation sample volumes may be accounted for.

The possibility of using L to estimate the dispersion parameter (μ) in the gamma drop size distribution is investigated. We find that including drop oscillations is essential for this application, otherwise there could be biases in retrieved μ of up to ≈ 8. Preliminary results in rainfall are presented. In a convective rain case study, our estimates show μ to be substantially larger than 0 (an exponential DSD). In this particular rain event, rain rate would be overestimated by up to 50% if a simple exponential DSD is assumed.

1

1. Introduction

The co-polar correlation coefficient, ρ_{hv}, between horizontal (H) and vertical (V) polarisation radar signals is a measure of the variety of hydrometeor shapes in a pulse volume. It is therefore useful for applications such as identifying the melting layer (Caylor and Illingworth 1989; Brandes and Ikeda 2004; Tabary et al. 2006; Giangrande et al. 2008), ground clutter (e.g. Tang et al. 2014), rain-hail mixtures (Balakrishnan and Zrnic 1990) and interpreting polarimetric signatures in ice (e.g. Andrić et al. 2013), and potentially the retrieval of the drop size distribution (DSD). The standard deviations of differential reflectivity (Z_{DR}) and differential phase shift (ϕ_{dp}) are both functions of ρ_{hv} (Bringi and Chandrasekar 2001). Therefore, ρ_{hv} dictates both the quality of dual polarisation measurements and their weighting in hydrometeor classification schemes (Park et al. 2009). In rainfall, ρ_{hv} is typically 0.98—1. Giangrande et al. (2008) use data where $\rho_{hv} < 0.97$ to identify the melting layer. For hail, ρ_{hv} can be much lower due to the effects of Mie scattering. At present, quantitative use of ρ_{hv} is hampered by a lack of rigorous confidence intervals accompanying the ρ_{hv} estimates. Error estimates are available adopting an empirical approach (Illingworth and Caylor 1991) or a linear perturbation technique (Liu et al. 1994; Torlaschi and Gingras 2003), both of which implicitly assume a Gaussian probability distribution for the ρ_{hv} samples. We will show that the distribution of ρ_{hv} samples is in fact non-Gaussian and highly negatively skewed.

Natural rain drop size distributions can be described by a gamma distribution (Ulbrich 1983):

$$N(D) = N_0 D^\mu \exp\left[-\frac{(3.67 + \mu)}{D_0}D\right] \tag{1}$$

where D is the equivalent spherical drop diameter, N_0 is the intercept parameter, D_0 is the median volume drop diameter and μ is the dispersion parameter (a measure of the drop size spectrum shape). If $\mu = 0$, by exploiting the relationship between drop diameter and drop

axis ratio, D_0 can be estimated using Z_{DR} (Seliga and Bringi 1976). Higher μ correspond to more monodisperse drop size distributions. Since ρ_{hv} is sensitive to variations in drop shape, it can in principle be used to estimate μ (Jameson 1987), knowledge of which could improve dual polarisation and dual frequency (e.g. the Global Precipitation Measurement satellite) rain rate estimates. Figure 1 shows rain rate (R) per unit radar reflectivity (Z) as a function of Z_{DR} for simulated Gamma distributions with $\mu = $ -1, 0, 2, 4, 8, 12 and 16. The rain rate is sensitive to variability in the shape of the drop size spectrum; uncertainty in μ alone could introduce an error in the retrieved rain rate of up to 2.5 dB (almost a factor of 2) for a given pair of Z and Z_{DR} observations.

It is difficult to obtain reliable estimates of μ from observations. Disdrometers suffer from undersampling of large drops, which cause μ values that are derived from the 3rd, 4th and 6th moments of the drop size distribution to be biased high (Johnson et al. 2014). Furthermore, disdrometers also undercount the number of drops < 0.5 mm (Tokay et al. 2001), which can also introduce a bias in estimates of μ. Estimating DSD parameters using radar is therefore preferable, due to the very large number of drops being sampled. Wilson et al. (1997) made radar observations dwelling in rain at elevation angles above 20° and report that the difference in the mean Doppler velocity at H and V polarisations provides an estimate of μ, which were in the range of 1 to 11, and, once Z_{DR} exceeded 0.5 dB, all the values were above 4. Doppler spectra of rain at vertical incidence with multiple wavelength radars, including wind profiler frequencies that respond to the clear air motion have been utilised to estimate μ (Williams 2002; Schafer et al. 2002). These experiments find μ ranges between 0 and 18, but is typically 0—6. Unal (2015) fits observed Doppler spectra to theoretical drop spectra at S-band, and retrieves μ in the range of -1—5. The disadvantage of these techniques is that they use high elevation angles; for operational monitoring of surface rainfall, measurements at low elevation angles are preferable. This motivates the use of ρ_{hv} to derive μ in rainfall. Illingworth and Caylor (1991) and Thurai et al. (2008) inferred μ from the decrease in ρ_{hv} as Z_{DR} increases. The difficulty here is that any mis-matches in the H and V beams

₇₅ will introduce an uncorrelated noise component, so that even for perfectly spherical drizzle

₇₆ droplets, where the "true" ρ_{hv} is unity, the radar will always detect a value less than one (we

₇₇ will call this maximum obtainable level of ρ_{hv} "f_{hv}^{max}", see Section 5). From measurements in

₇₈ rain at short range, Illingworth and Caylor (1991) inferred μ values, which if corrected with

₇₉ an estimate of f_{hv}^{max} were in the range 0—2, but even for long dwells the estimated errors

₈₀ in μ were quite large. Thurai et al. (2008) analysed ρ_{hv} measurements from an operational

₈₁ radar and obtained estimates of μ in the range of 1—3, however their approach relies on

₈₂ empirically derived relationships between ρ_{hv} and DSD widths from 2 dimensional video

₈₃ disdrometer (2DVD) measurements. Furthermore, the technique is only valid for intense

₈₄ rain ($Z_{DR} \geq 2$ dB and $\rho_{hv} < 0.98$).

₈₅   The aim of this paper is to define a new variable, $L = -\log_{10}(1 - \rho_{hv})$, that has Gaussian

₈₆ error statistics with a width predictable from the number of independent radar pulses. This

₈₇ can be readily estimated by using the observed Doppler spectral width (σ_v). We will then

₈₈ present measurements of L in rainfall as a function of Z_{DR}, and retrieve estimates of μ by

₈₉ comparing these with predicted L and Z_{DR} for various three-parameter gamma distributions.

₉₀ The possibility of using this technique to retrieve μ using operational radars is then discussed.

₉₁ # 2. The Co-Polar Correlation Coefficient (ρ_{hv})

₉₂ ρ_{hv} is defined as (Doviak and Zrnic 2006):

$$\rho_{hv} = \frac{\langle S_{VV} S_{HH}^* \rangle}{\sqrt{\langle |S_{HH}|^2 \rangle \langle |S_{VV}|^2 \rangle}} \tag{2}$$

₉₃ where $\langle S_{HH} \rangle$ and $\langle S_{VV} \rangle$ are the co-polar elements of the backscattering matrix averaged

₉₄ over an ensemble of scatterers for the H and V polarisations respectively, and * indicates the

₉₅ complex conjugate. It can be estimated by correlating successive power or complex (I and

₉₆ Q) measurements. Examples of power time-series in (a) drizzle and (b) heavier rainfall from

the 3 GHz Chilbolton Advanced Meteorological Radar (CAMRa) are shown in figure 2. The radar is a coherent-on-receive magnetron system, transmitting and receiving alternate H and V polarised pulses with a pulse repetition frequency (PRF) of 610 Hz. A cubic polynomial interpolation is used to estimate the H power at the V pulse timing and the V power at the H pulse timing. Its narrow one-way half power beamwidth (0.28°) makes it capable of very high resolution measurements. The full capabilities of this radar are discussed in Goddard et al. (1994). The observed fluctuating signals in Figure 2 are caused by the superposition of the backscattered waves from each drop in the sample volume; the rate of fluctuation is determined by the Doppler spectral width. For drizzle, since the drops are spherical, $Z_{DR} = 0$ dB, and the H and V signals are almost perfectly correlated: $\rho_{hv} = 0.995$. For heavier rainfall, a systematically lower V power is received ($Z_{DR} = 1.1$ dB), and the signals are visibly less correlated ($\rho_{hv} = 0.987$), due to the broader axis ratio distributions in the sample volume.

These estimates of ρ_{hv} are derived from a finite number of reshufflings, and therefore there is some uncertainty in them. In what follows, we quantify this uncertainty.

3. Theoretical Measurement Error in Estimated Correlation of Time-Series

Figure 3a shows the distribution of estimates of the correlation coefficient, $\hat{\rho_{hv}}$ (calculated from a finite length time-series), as distinct from the "true" co-polar correlation coefficient, $\overline{\rho_{hv}}$ (that would be measured for a time-series of infinite length). The data was collected during a 1.5° elevation dwell in drizzle ($Z_{DR} < 0.1$ dB), with very high SNR (> 40 dB) on 6 February 2014. Each $\hat{\rho_{hv}}$ is calculated from 64 H and V pulse pairs (0.21s dwell) from a single 75 m range gate with $\sigma_v = 1.1 \pm 0.1$ ms $^{-1}$. The distribution of $\hat{\rho_{hv}}$ has a peak that is close to $\overline{\rho_{hv}}$ (which is < 1, see Section 5d), but exhibits a very long tail at lower $\hat{\rho_{hv}}$, while there are no data with $\hat{\rho_{hv}} > 1$. Clearly, this distribution is not Gaussian and the negative

5

skewness will negatively bias the mean of many $\hat{\rho_{hv}}$ samples compared to the true value of ρ_{hv}.

Fisher (1915) states that sample correlation coefficients ($\hat{\rho}$) of a "true" correlation coefficient ($\overline{\rho}$) calculated from a finite number of Gaussian random variables are skewed for $\overline{\rho} \neq 0$. However, the variable:

$$\hat{F} = \frac{1}{2} \ln \left(\frac{1 + \hat{\rho}}{1 - \hat{\rho}} \right) \tag{3}$$

is Gaussian, with a mean of:

$$\bar{F} = \frac{1}{2} \ln \left(\frac{1 + \overline{\rho}}{1 - \overline{\rho}} \right) \tag{4}$$

and standard error of:

$$\sigma_F = \frac{1}{\sqrt{N - 3}} \tag{5}$$

where N is the number of independent samples used to calculate $\hat{\rho}$.

This is directly applicable to estimates of the radar co-polar correlation coefficient, by realising that the I and Q samples that are used to estimate ρ_{hv} are Gaussian random variables (Doviak and Zrnic 2006). Noting that $\hat{\rho_{hv}}$ in meteorological targets is always close to unity so that fractional changes in $(1 - \hat{\rho_{hv}})$ are always much greater than $(1 + \hat{\rho_{hv}})$, Equation 3 can be written as:

$$\hat{F} \approx \frac{1}{2} \ln 2 - \frac{\ln 10}{2} \log_{10}(1 - \hat{\rho_{hv}}) \tag{6}$$

Since $\hat{F}$ is normally distributed, the quantity:

$$\hat{L} = -\log_{10}(1 - \hat{\rho_{hv}}) \tag{7}$$

is also normally distributed, with a mean:

$$\bar{L} = -\log_{10}(1 - \overline{\rho_{hv}}) \tag{8}$$

and standard deviation of:

$$\sigma_L = \frac{2}{\ln 10} \times \frac{1}{\sqrt{N_{IQ} - 3}} \tag{9}$$

for $N_{IQ} \gg 3$, where N_{IQ} is the number of independent I and Q samples used to calculate $\hat{\rho_{hv}}$. Despite having similar characteristics, L is preferred over the use of F as it has the convenient property that $\rho_{hv} = 0.9$, 0.99 and 0.999 correspond to $L = 1$, 2 and 3 respectively and therefore is more intuitive. Illingworth and Caylor (1991) plotted their $\hat{\rho_{hv}}$ data as $\log_{10}(1 - \hat{\rho_{hv}})$ and their histograms also appear Gaussian in shape. Figure 3b illustrates the effect of the transform $\hat{L} = -\log_{10}(1 - \hat{\rho_{hv}})$ on the distribution in Figure 3a. The histogram is now symmetrical, and bell shaped. A Gaussian curve with an equal mean and standard deviation to the $\hat{L}$ PDF is overplotted and is an excellent fit to the data, showing that the distributions are indeed Gaussian (and Quantile - Quantile plots, not shown here for brevity, confirm this).

To determine the number of independent I and Q samples, N_{IQ}, we consider the auto-correlation function for I and Q samples given by Doviak and Zrnic (2006):

$$R_{IQ}(nT_s) = \exp\left[-8\left(\frac{\pi\sigma_v nT_s}{\lambda}\right)^2\right] \tag{10}$$

where T_s is the time spacing between pulses of the same polarisation and nT_s is the total time lag. Following the definition of Papoulis (1965), the time to independence for I and Q samples for large N_{IQ} can be shown to be:

$$\tau_{IQ} = \frac{\lambda}{2\sqrt{2\pi}\sigma_v} \tag{11}$$

where λ is the radar wavelength and σ_v is the Doppler spectral width. This is a factor of $\sqrt{2}$ smaller than the more often used time to independence for reflectivity samples. The number

7

of independent I and Q pulses per ρ_{hv} sample can therefore be estimated by:

$$N_{IQ} = \frac{T_{dwell}}{\tau_{IQ}} = \frac{2\sqrt{2\pi}\sigma_v T_{dwell}}{\lambda} \tag{12}$$

where T_{dwell} is the dwell time.

The result (Equation 9) is significant as it shows that a confidence interval for any measurement of ρ_{hv} can be calculated solely in terms of the number of independent I and Q samples used to estimate it, which in turn can be readily estimated using the observed Doppler spectral width and Equation 12. Furthermore, when multiple samples of $\hat{L}$ are averaged, no bias is introduced to estimates of $\hat{\rho_{hv}}$ because of the non-linear transform. We expand this point in Section 4.

To estimate confidence intervals for measurements of $\hat{\rho_{hv}}$, one must:

- Apply the transform $\hat{L} = -\log_{10}(1 - \hat{\rho_{hv}})$

- Calculate the standard deviation of $\hat{L}$ using Equation 9.

- Apply the inverse transform $1 - 10^{-(\hat{L}\pm\sigma_L)}$ to obtain upper and lower confidence intervals (where σ_L will contain the true value 68% of the time and $2\sigma_L$ 98%).

More conveniently, one can simply transform $\hat{\rho_{hv}}$ data to $\hat{L}$ and use this for any subsequent analysis, with confidence intervals of $\hat{L} \pm \sigma_L$. This is the approach we follow in the rest of this paper. Although we are focusing on data with very high signal-to-noise (SNR) in this paper, the theory above should also be valid for weak SNR data, providing that noise introduced is also Gaussian in the I and Q samples.

This theoretical prediction was tested by comparing estimates of σ_L using data collected in homogeneous drizzle ($Z_{DR} < 0.1$ dB) with very good signal-to-noise (SNR > 40 dB). In drizzle, $\overline{L}$ is constant since the drops are spherical, and therefore any variation σ_L is due to the finite N_{IQ}. Pulse-to-pulse H and V powers were recorded, and time series of various lengths between 0.2—30 s were constructed from these data and used to compute

8

178 the corresponding N_{IQ} and L values. Data was binned by N_{IQ}, and the standard deviation,

179 σ_L, were computed for each bin. Figure 4 shows how σ_L decreases as N_{IQ} is increased over

180 more than two orders of magnitude. σ_L is slightly overestimated for $N_{IQ} \approx 10$, and the data

181 is in excellent agreement to that predicted by Equation 9 for $N_{IQ} > 30$.

4. Comparison with Existing Error Statistics

183 We now compare these new error statistics with existing methods in the literature. From

184 observations of ρ_{hv} in rain, the bright-band and ice, Illingworth and Caylor (1991) derived

185 empirically the relationship between their mean $\hat{\rho_{hv}}$ estimates and their standard deviation:

$$\sigma_{\rho_{hv}}^{IC} \simeq \frac{1.25(1 - \hat{\rho_{hv}})}{\sqrt{n}} \tag{13}$$

186 where n is the number of 0.2 s time-series they used to estimate the mean ρ_{hv}. Using a linear

187 perturbation technique, Torlaschi and Gingras (2003) derive the following equation for the

188 standard deviation on a ρ_{hv} measurement:

$$\sigma_{\rho_{hv}}^{TG} = \frac{1 - \bar{\rho_{hv}}^2}{\sqrt{2N_I}} \tag{14}$$

189 where N_I is the number of independent radar reflectivity samples used in its estimation. Note

190 that $\overline{\rho_{hv}}$ in Equation 14 is the "true" correlation coefficient one is attempting to measure

191 (rather than the measured value, $\hat{\rho_{hv}}$). This equation represents the standard deviation

192 for infinite SNR conditions, and is valid for simultaneous or accurately interpolated H and

193 V sampling. Neither of these techniques are ideal, relying on either knowing a-priori the

194 true correlation coefficient one is attempting to measure (Torlaschi and Gingras 2003), or a

195 number of time-series (Illingworth and Caylor 1991), not the number of independent pulses.

196 It is not possible to compare the method of Illingworth and Caylor (1991) with our proposed

197 method as σ_v for their data is unknown, and therefore the number of independent pulses in

198 their time-series cannot be quantified. Figure 5a shows the errors on $\hat{\rho_{hv}}$ calculated using our

9

new method compared to those calculated using the linear perturbation method of Torlaschi and Gingras (2003) as a function of N_{IQ} in rain ($\overline{\rho_{hv}} = 0.98$). The magnitudes of the upper confidence bounds are largely similar, however, for all N_{IQ} the lower confidence interval is higher for Torlaschi and Gingras (2003) (i.e smaller deviations from $\overline{\rho_{hv}}$ are predicted), due to the asymmetric nature of the new confidence intervals on $\hat{\rho_{hv}}$. The largest difference is for small N_{IQ}. As N_{IQ} increases, both the upper and lower confidence intervals for each method converge. Although Figure 5a serves as a useful illustration of the difference between the methods, they are not strictly comparable in practice: the error calculation of Torlaschi and Gingras (2003) relies on knowledge of $\overline{\rho_{hv}}$ which in reality is unknown. Conversely, the new method requires no a-priori knowledge of $\overline{\rho_{hv}}$, and so is of much greater practical use.

Figure 5b illustrates the theoretical bias introduced by averaging many short samples of $\hat{\rho_{hv}}$, rather than $\hat{L}$, in rain ($\overline{\rho_{hv}} = 0.98$). This bias is significant for small N_{IQ}. For example, when $N_{IQ} = 10$, the bias on $\hat{L}$ is 0.1, which is significant for the purpose of estimating μ in rainfall; this bias in L could lead to an underestimate of μ of ≈ 8 at $Z_{DR} = 2$ dB (see figure 8). It is not important whether spatial or temporal averaging is used to increase the number of independent I and Q samples, as long as $\overline{\rho_{hv}}$ does not vary substantially over the scales considered.

In summary, confidence intervals that rely on the linear perturbation method overestimate the precision of ρ_{hv} measurements, and require knowledge of the "true" ρ_{hv} one is attempting to measure. Fundamentally, failure to use the transform L when averaging short time-series will lead to significant biases in correlation coefficient estimates. This is particularly important for operational ρ_{hv} applications that typically use very short dwell times (discussed in Section 8a), and would lead to a significant bias in retrievals of μ in rain.

5. Practical measurement of ρ_{hv}

To fully exploit our new error estimates, and retrieve rain DSDs, some practical consid-
erations for the measurement of ρ_{hv} must first be considered.

a. Effect of alternate sampling

When estimating the correlation coefficient, the non-simultaneous transmission and re-
ception of H and V pulses must be accounted for. Assuming a Gaussian autocorrelation
function to correct for this staggered sampling (Sachidananda and Zrnic 1989) can lead to
unphysical samples where $\hat{\rho_{hv}} > 1$ (Illingworth and Caylor 1991). In our analysis, we employ
a cubic polynomial interpolation to obtain H and V power estimates at the intermediate
sampling intervals (Caylor 1989), which is very effective. We find that the interpolation
scheme works well: for drizzle with $\overline{L} = 2.4$, we observe that average values of $\hat{L}$, binned
by σ_v, are constant to within ± 0.02 as σ_v varies between 0.1—2 ms^{-1}. This is evidence
of successful interpolation, since there is no systematic trend to lower L values at higher
spectral widths.

b. Signal-to-noise ratio

The addition of noise to the received signals acts to reduce the correlation between H
and V time-series. The reduction factor, f, has been shown (Bringi et al. 1983) to vary
predictably as:

$$f = \frac{1}{\left(1 + \frac{1}{SNR_H}\right)^{\frac{1}{2}} \left(1 + \frac{1}{SNR_V}\right)^{\frac{1}{2}}} \tag{15}$$

for simultaneous (or accurately interpolated) H and V sampling, where SNR_H and SNR_V
are the signal-to-noise ratios for the H and V polarisations respectively. This was verified by

²⁴² Illingworth and Caylor (1991) with measurements of ρ_{hv} in drizzle. Whilst it is in principle

²⁴³ possible to correct for the presence of noise using this equation, due to the high degree of

²⁴⁴ precision required in this work, only data with SNR > 34 dB are included in our analysis,

²⁴⁵ which corresponds to a maximum achievable ρ_{hv} measurement of 0.9996. However, instru-

²⁴⁶ mental effects (described in Section d below) will have the same effect of adding uncorrelated

²⁴⁷ noise, and so in practice this maximum value is never reached.

²⁴⁸ *c. Effect of phase error*

²⁴⁹ To avoid a bias in $\hat{\rho_{hv}}$ due to random phase error from our magnetron system (Liu et al.

²⁵⁰ 1994), we cross correlate the power of the received echoes as opposed to the complex I and

²⁵¹ Q signals, and take the square root, following Illingworth and Caylor (1991).

²⁵² *d. Instrumental effects*

²⁵³ Even in drizzle with very high SNR, antenna imperfections and other effects such as

²⁵⁴ irregular magnetron pulse timing and pulse shape reproducibility will cause measured ρ_{hv} to

²⁵⁵ always be < 1 (Illingworth and Caylor 1991; Liu et al. 1994) as effectively they cause the H

²⁵⁶ and V pulses to sample slightly different volumes. Here, we propose a method to quantify

²⁵⁷ and account for this bias, analogous to the SNR factor (Equation 15) suggested by Bringi

²⁵⁸ et al. (1983). We consider the H and V echoes to consist of two parts: a common sample

²⁵⁹ volume, and parts of each sample volume which are unique to a particular polarisation. By

²⁶⁰ treating the former as "signal" and the latter as unwanted "noise", we obtain an equation

²⁶¹ similar to Equation 15. Full details are provided in the appendix. The practical upshot

²⁶² is that the measured ρ_{hv} is the "true" ρ_{hv} multiplied by some dimensionless factor, f_{hv}^{max},

²⁶³ relating to how well matched the H and V sample volumes are. For spherical drops, $\overline{\rho_{hv}}$

²⁶⁴ should be unity. The estimates of $\overline{\rho_{hv}}$ for all such data should therefore be equal to f_{hv}^{max}.

²⁶⁵ When comparing observations with simulated ρ_{hv}, we multiply each of the predicted values

12

by f_{hv}^{max} so that they are directly comparable to the observations. ρ_{hv} has been measured in drizzle ($Z_{DR} < 0.1$ dB) for a large number of samples on several days. Typically, f_{hv}^{max} is ≈ 0.996, but varies by $\pm$ 0.001 from day to day, which we suggest is the result of slightly irregular magnetron pulse timing and shape reproducibility for the CAMRa system, which may be temperature dependent. For this reason, f_{hv}^{max} has been determined individually for each case.

6. Using L and Z_{DR} to Estimate μ in Rainfall

We now attempt to use our high-precision measurements of L to retrieve μ estimates in rainfall. The independence of (D_0, μ) and (L, Z_{DR}) on the drop number concentration means that a single L and Z_{DR} observation pair corresponds to a unique D_0 and μ value. In order to forward model L and Z_{DR} for various gamma distributions, we must first assume an appropriate drop shape model.

a. Mean Drop Shapes

There are numerous drop shape parameterisations in the literature. Here, we examine drop axis ratios and diameters from the recent experiments of Thurai and Bringi (2005), Szakáll et al. (2008) and the 4th order polynomial fit to many experiments given by Brandes et al. (2002). Figure 6a shows the mean axis ratio as a function of drop diameter, for each of these models. The Thurai and Bringi (2005) data suggests that mean drop shapes are slightly prolate for $D < 1$ mm, although it is in the margin of measurement error that the drops are spherical (Beard et al. 2010). Since it is known that drops become spherical as their diameter tends to 0 mm due to surface tension, our fit to the data is adapted so that drops < 1 mm are precisely spherical.

To choose the best mean drop shape model, a 5 hour dwell was made with CAMRa at a 1.5° elevation angle over a nearby Joss-Waldvogel RD-80 impact disdrometer (approximately

13

290 7 km away) in a frontal rain band on 25 April 2014. The disdrometer measures drop sizes in

291 127 size bins from 0.3 to 5.0 mm. The instrument is regularly calibrated by the manufacturer

292 and rain rate estimated with this instrument agrees very well with that from a co-located

293 rain gauge. Radar measurements of Z_{DR} are calibrated regularly (to within ±0.1 dB) by

294 making observations of drizzle (low Z), which we know to have a Z_{DR} value of 0 dB. The

295 range resolution of the radar measurements is 75 m, and averaged to 30 s to match the

296 integration time used by the disdrometer to estimate the DSD parameters. At this elevation

297 angle, the radar was sampling rain at a height of 183m above the disdrometer. Figures

298 6b—d show the observed radar measurement from the closest gate to the disdrometer, and

299 the corresponding disdrometer Z_{DR} values calculated using the Thurai and Bringi (2005),

300 Szakáll et al. (2008) and Brandes et al. (2002) drop shape models respectively. The Szakáll

301 et al. (2008) axis ratios are systematically smaller compared to both of the other models for

302 almost all D. Using this model makes the disdrometer estimates of Z_{DR} always larger than

303 the radar estimates. Thurai and Bringi (2005) and Brandes et al. (2002) agree for $D = 2$—7

304 mm, after which the axis ratios of Thurai and Bringi (2005) are closer to those of Szakáll

305 et al. (2008). Therefore, radar and disdrometer Z_{DR} for the Thurai and Bringi (2005) and

306 Brandes et al. (2002) models largely agree, apart from $Z_{DR} \lesssim 0.4$ dB. The largest differences

307 between these models occurs for $D < 2$ mm. Here, Szakáll et al. (2008) and Brandes et al.

308 (2002) predict more oblate drops than Thurai and Bringi (2005).

309 The Szakáll et al. (2008) model produces the largest radar-disdrometer overall bias of

310 ≈ 0.23 dB. The biases from Brandes et al. (2002) for Z_{DR} bins of 0.2, 0.4 and 0.6 dB ($\pm$

311 0.1 dB bin width) are 0.09, 0.16 and 0.13 dB respectively. For Thurai and Bringi (2005),

312 they are only 0.04, 0.08 and 0.09 dB respectively, and are very similar to Brandes et al.

313 (2002) at higher Z_{DR}. These reduced biases at low Z_{DR} suggest that the experimental

314 results of Thurai and Bringi (2005) best represent natural raindrop shapes. We therefore

315 chose this model in our analysis. It is unclear why the very small residual difference between

316 radar and disdrometer estimates of Z_{DR} using the Thurai and Bringi (2005) shape model is

14

observed. Some possible explanations are that the radar calibration is slightly out causing a systematic underestimation, the small sampling volume of the disdrometer could be biasing Z_{DR}, or there could be residual error in the mean drop shape model. However, this very small difference is unimportant for retrievals that follow.

b. Drop Oscillations

Drop oscillations increase the variety of shapes within a radar pulse volume at any given time. This means that the $\overline{L}$ we are attempting to estimate will be lower than that predicted by modelling only the mean drop axis ratios for drops of a given size. In order to account for this, we must parameterise these drop oscillations. In the Thurai and Bringi (2005) experiment, artificial rain drops were created from a hose and allowed to fall 80 m from a bridge before drop axis ratio and counts were measured with a 2D video disdrometer (2DVD) on the valley floor. This fall distance is more than sufficient to allow the drops to achieve steady state oscillations, and so the standard deviations of axis ratios measured in this experiment are interpreted as drop oscillation amplitudes. However, the large standard deviations of the axis ratios for $D < 2$ mm are likely artificial, caused by the finite resolution of the 2DVD instrument (Beard et al. 2010). Since drop oscillations are thought to originate from vortex shedding (Beard et al. 2010) which increases as a function of drop size, the magnitude of oscillations should decrease eventually to zero as the drop diameter tends to 0 mm. Beard and Kubesh (1991) suggest that resonant drop oscillations occur for drop sizes between 1.1 and 1.6 mm, however more recent measurements from the Mainz wind tunnel show that amplitudes of the axis ratios for these drop sizes were less than 0.025 (Szakáll et al. 2010). For this reason, the polynomial fit to oscillation amplitude data from the Mainz wind tunnel (Szakáll et al. 2010) is used for $D < 2$ mm, which has the desired reduction in oscillation amplitude for small drops [1]. For $D > 2$ mm, we revert to the more

---

[1] Equation 1 in Szakáll et al. (2010) does not agree with the fit in Figure 3 (black line). By digitising the Mainz wind tunnel data, we calculate that Equation 1 should in fact be $1.8 \times 10^{-3} D_0{}^2 + 1.07 \times 10^{-2} D_0$

15

statistically robust drop oscillations from Thurai and Bringi (2005). Since the oscillations are aerodynamically induced, with an amplitude only a function of the drop size, they should not vary with environmental conditions. In our analysis, the oscillations were included by integrating over Gaussian PDFs of axis ratios (Thurai and Bringi 2005) in our Gans theory computations. Figure 7 shows the effect of oscillations on computed L and Z_{DR} for values of $\mu = $ -1 (black lines), $\mu = 16$ (grey lines). Including drop oscillations for the purpose of estimating μ becomes increasingly important with increasing Z_{DR}; the difference between L at $\mu = 16$ computed with and without oscillations is as large as an equivalent change in μ of ≈ 8. We find that the modification of the oscillation magnitudes for drop diameters < 2 mm has a relatively small impact (< 0.01) on predicted L for Z_{DR} larger than 0.8 dB where we attempt retrievals of μ. However, we find that the use of Szakáll et al. (2010) oscillations for all drop diameters has a large impact on predicted L values (for $\mu = $ -1, L is ≈ 0.1 lower). This is potentially important for retrievals of μ.

Comparatively large amplitude (but short lived, lasting less than ≈ 0.4 s) collision induced oscillations can also occur (Szakáll et al. 2014). Rogers (1989) estimate that the collision rate for an average rain drop in a 55 dBZ rain column is ≈ 1 min^{-1}. This would imply that rain drops (even in very heavy rainfall) spend an almost negligible fraction of time ($\approx 0.5\%$) affected by collision-induced oscillations . Rain drop clustering increases the likelihood of these collisions (Jameson and Kostinski 1998). For rain rates of around 10 mm hr^{-1} (comparable to those presented in the following case studies), McFarquhar (2004) estimate the collision rate to be ≈ 5 min^{-1}, implying drops are affected only 3% of the time. For very large rain rates (100 mm hr^{-1}), this fraction increases to 6% as the collision rate approximately doubles to 10 min^{-1}. Consequently, their impact on L measurements is likely to be small and can be ignored, other than for exceptional rain rates (Thurai et al. 2013).

Figure 8 shows how L varies as a function of Z_{DR} for gamma distributions with $\mu = $ -1, 0, 2, 4, 8, 12 and 16 computed using Gans theory with the drop shape and oscillation model discussed above. Note that lines of constant μ diverge with increasing Z_{DR}. For $Z_{DR} \gtrsim$

16

0.5 dB, it becomes possible to distinguish μ, given the typical error on an L measurement (shown in Figure 9).

7. μ Retrieval Case Studies

We now estimate μ using measurements of L and Z_{DR} for stratiform rain case studies on 31 January, 25 April and 25 November 2014, and a convective case study on 22 May 2014. Typical rain rates for each of these case studies can be found in Table 1. Dwells were made at an elevation angle of 1.5°. Strict data quality filters were applied: SNR > 34 dB, linear depolarisation ratio (LDR) < −27 dB (close to the limit of cross-polar isolation) to ensure no melting particle contamination or ground clutter and range > 5 km to avoid near-field effects. Theoretical L and Z_{DR} were computed using Gans theory using the drop shape and oscillation model discussed in Section 6 (see Figure 8). Observations were averaged from 10 to 30 s and from range gates of 75 to 300 m to increase the measurement precision of L. At each gate, the most likely pair of μ and D_0 given the observed L and Z_{DR} values was obtained by selecting the closest point in a look-up table of Gamma DSD calculations. Figure 9a shows the observed L binned every 0.02 and Z_{DR} binned every 0.05 dB for the example of 25 November 2015. Overlayed are lines of constant μ = -1, 0, 2, 4, 8, 12 and 16. Figure 9b is the same distribution normalised to sum to 1 for each Z_{DR} bin. The f_{hv}^{max} on this day was calculated to be 0.9963 (see Section 5d). The observations of L and Z_{DR} are generally well contained within the expected range. The median error on $\hat{L}$ is $\sigma_L \approx$ 0.025, and is shown as a representative error bar in Figure 9. A comparison of these data with disdrometer measurements from Williams et al. (2014) is included. In this experiment, the mass spectrum mean diameter (D_m) and mass spectrum standard deviation (σ_m) were measured using a 2DVD. A $\sigma_m - D_m$ fit was derived from 18969 1-minute drop spectra (which can readily be converted to a $\mu - D_0$ fit). This was in turn used to predict a $L - Z_{DR}$ relationship, shown by the grey dashed line. L and Z_{DR} were also predicted using the

17

393 proposed $\mu - \Lambda$ relationship of Cao et al. (2008), also derived from a 2DVD, where:

$$\Lambda = \frac{3.67 + \mu}{D_0} \tag{16}$$

394 This is shown by the black dashed line.

395   The median and inter-quartile range of retrieved μ per Z_{DR} bin for this day is shown in

396 Figure 10. The median retrieved μ is 5 at $Z_{DR} = 0.8$ dB, increasing to 8 for $Z_{DR} = 1.6$ dB.

397 There is significant spread in retrieved μ values, containing contributions from measurement

398 uncertainty on L, as well as "true " microphysical variability. The impact of changes in L

399 on retrieved μ is non-linearly related to μ; σ_L contributes more to retrieved μ variability

400 for more monodosperse (higher μ) DSDs, compared to more polydisperse (lower μ) DSDs.

401 Conversely, the contribution of σ_L to retrieved μ variability decreases as Z_{DR} increases, as

402 the dual polarisation signature is larger and μ is more easily distinguishable (see Figure 8).

403 To estimate the contribution that the uncertainty on L measurements makes to this observed

404 variability, μ was retrieved using the median $L \pm$ the representative uncertainty depicted

405 in Figure 9. This was then compared to the inter-quartile range of the retrieved μ for each

406 Z_{DR} bin. For Z_{DR} bins of 0.8, 1, 1.2, 1.4 and 1.6 dB, we estimate that 88%, 66% 32%, 31%

407 and 27% of the variability respectively can be attributed to σ_L. For $Z_{DR} > 1$ dB, most of

408 the variability seen in Figure 10 can be attributed to "true" microphysical variability.

409   Figure 11 shows a comparison with retrieved μ for all of the case studies collected. Each

410 of the dwells in January, April and November were made in stratiform rain, whereas the

411 May case study contains dwells from convective rain. Overlayed are predicted mean μ values

412 (solid grey) and upper and lower bounds that contain 55% of the measurements (dashed

413 grey) of Williams et al. (2014) as a function of Z_{DR} from the disdrometer measurements.

414 The solid black line shows the predicted $\mu - Z_{DR}$ using the $\mu - \Lambda$ relationship of Cao et al.

415 (2008). There is a large spread in the radar retrieved median μ values from case to case.

416 Each median μ estimate is from a very large number of retrieved μ estimates, such that the

417 standard error is smaller than the markers themselves, and so is not shown. The values of

18

418 retrieved μ in January are ≈ 0, close to an exponential DSD for all Z_{DR} smaller than 1.1 dB.
419 This is below that predicted by Williams et al. (2014), but agrees well with μ predicted by
420 Cao et al. (2008). Interestingly, the case studies of April and November show μ increasing
421 with Z_{DR} between 0.5 dB and 1.5 dB, compared to the trend seen by Williams et al. (2014)
422 and Cao et al. (2008) towards an exponential DSD. The retrieved median μ values from
423 the May case study, although agreeing with the decreasing trend with Z_{DR}, are significantly
424 above the Cao et al. (2008) predictions and the upper bound of μ from Williams et al. (2014).
425 Our retrieval suggests that in this case, the rain rate would be overestimated by almost 2
426 dB if an exponential DSD or the fit of Cao et al. (2008) is assumed. Whereas the μ values
427 are not outside the full range of data measured by Williams et al. (2014), the use of the
428 proposed $\mu - D_m$ relationship would cause an overestimate of ≈ 1 dB (see Figure 1).

8. Discussion

430   Our retrievals of μ made using ρ_{hv} and Z_{DR} are typically larger than the radar estimates
431 of μ of between 1—3 by Thurai et al. (2008) and 0—2 of Illingworth and Caylor (1991).
432 Perhaps this is not surprising, given that the imperfect co-location of the H and V sample
433 volumes was unaccounted for, and their $\hat{\rho_{hv}}$ would have been biased low due to averaging ρ_{hv}
434 rather than L, both of which are accounted for in our data . Furthermore, Illingworth and
435 Caylor (1991) do not include drop oscillations in their retrievals, which will have led to a
436 significant underestimate of μ. Whereas there is some agreement of the magnitudes of μ for
437 $Z_{DR} < 1$ dB with predicted Williams et al. (2014) and Cao et al. (2008) values, the apparent
438 opposite trend towards more monodisperse distributions is consistent among 3 of the 4 case
439 studies. For the retrieved μ to agree with the trend predicted by Williams et al. (2014) or
440 Cao et al. (2008), a reduction in the drop oscillation amplitudes for smaller drops would be
441 required so that predicted L values are higher. However, this would not explain the difference
442 between the May retrieval results and the predicted μ from disdrometer measurements; we

19

estimate that it would require oscillations that are at least an order of magnitude *larger* to bring these median μ estimates into agreement with Williams et al. (2014) or Cao et al. (2008). An incorrect parameterisation of the drop oscillations alone is unlikely to be able to account for the disagreement with Williams et al. (2014) and Cao et al. (2008), however, to better establish the accuracy of the technique, a better quantification of raindrop oscillations is desirable.

μ estimates derived using radar are sensitive to higher moments of the DSD, whereas disdrometer estimates tend to use lower moments of the DSD (Cao and Zhang 2009). This could be partly responsible for the differences between the radar and disdrometer estimated μ values. If the DSD shape is not perfectly described by Equation 1, the "effective " μ which is derived may be different even if the underlying DSD shape is the same. It is also possible that what we have captured is simply natural variability of the DSD in different types of rainfall (i.e convective and stratiform), and there is not a universal $\mu - D_0$ relationship. More case studies are needed to gather a statistical understanding of the behaviour of μ using this retrieval method.

a. *Implications for Operational Use of L*

Operational radar networks favour the use of rapid scan rates to maximise sample frequency and total sample volume. For UK Met Office radars observing rain with 1 ms^{-1} Doppler spectral width, each gate contains $N_{IQ} \approx 11$ ($\sigma_L \approx 0.3$). Clearly, many more N_{IQ} are needed than are available for individual gate estimates of μ. Greater measurement precision can be achieved by averaging (with the confidence interval computed using the aggregated number of independent I and Q samples), and assuming μ is spatially conserved over the chosen averaging area. To obtain a μ estimate over approximately 1 km^2, for example, would require the averaging of 2 rays and 10 gates (at a range from the radar of 30 km); this L estimate would be calculated using $N_{IQ} = 220$ ($\sigma_L \approx 0.058$). Whereas this may not be sufficient to distinguish μ to as high a resolution as our retrieval (which uses long

20

469 dwells and $N_{IQ} > 1000$), this will at least be able to decipher whether μ is 'high' or 'low'.

470 Practically, as illustrated in Figure 1, this may be all that is necessary to offer improved rain

471 rate estimates; it is relatively unimportant whether μ is 8 or 16, but it is very important to

472 know if it is 0 or 4. Therefore, this method could (with sufficient care to ensure only rain

473 echoes and good SNR) allow for improved rain rates using Z, Z_{DR} and L compared to only

474 Z and Z_{DR}.

475   For the typical σ_L used in these calculations, we can approximate the error on the re-

476 trieved rain rate by considering the contribution of σ_L to the uncertainty in μ. For a 'typical'

477 μ of 6, the range of retrieved μ is $\approx \pm 4$. By referring to Figure 1, we can see that this

478 corresponds to a difference in rain rate of ± 0.5 dB, or $\pm 12.5\%$. The impact of uncertainty

479 in μ on rain rate is almost constant for all Z_{DR} (each of the μ lines are approximately parallel

480 in Figure 1 for $Z_{DR} \gtrsim 0.5$ dB). Therefore, this error will decrease for higher rain rates as the

481 contribution of σ_L to uncertainty in μ decreases as a function of Z_{DR}.

9. Conclusions

483   In this paper, a new variable $L = -\log_{10}(1 - \rho_{hv})$ is defined that is Gaussian distributed

484 with a width predictable by the number of independent I and Q samples, which in turn

485 can be estimated using the Doppler spectral width. This allows, for the first time, the

486 construction of rigorous confidence intervals on each ρ_{hv} measurement. The predicted errors

487 using this new method were verified using high quality measurements in drizzle from the

488 Chilbolton Advanced Meteorological Radar.

489   Importantly, the proposed method is of much greater practical use than the linear per-

490 turbation error estimation method, as it does not require knowledge of the unknown "true"

491 ρ_{hv} that one is trying to estimate. The method works for both simultaneous or accurately

492 interpolated alternate sampling. However, it does not work for alternate estimators which

493 rely on the Gaussian autocorrelation function to estimate the zero-lag correlation between

$_{494}$ H and V pulses (Sachidananda and Zrnic 1989), where ρ_{hv} estimates can be > 1.

$_{495}$ A new technique to account for the imperfect co-location of H and V sampling vol-

$_{496}$ umes on ρ_{hv} measurements is presented. The impact of drop oscillations on the observed L

$_{497}$ measurements was shown to be significant; omitting oscillations from our Gans simulations

$_{498}$ leads to an underestimate of retrieved μ of ≈ 8. We further show that failure to use L over

$_{499}$ ρ_{hv} measurements when averaging can lead to a significant bias low in ρ_{hv} estimates (and

$_{500}$ consequently μ), particularly for very short dwell times such as those used operationally.

$_{501}$ High-precision measurements of L and Z_{DR} in rainfall are then used to estimate μ in

$_{502}$ the gamma DSD for four case studies. We find that our estimates of μ in stratiform rain

$_{503}$ somewhat agree in magnitude with those from disdrometer studies for small Z_{DR}, but there

$_{504}$ appears to be a tendency to more monodisperse DSDs between $Z_{DR} = 0.8$ and 1.5 dB, unlike

$_{505}$ the trend towards an exponential distribution suggested by disdrometer measurements. The

$_{506}$ convective case study does display this trend toward lower μ as Z_{DR} increases, but the

$_{507}$ magnitude of μ remains much larger than predicted by disdrometer measurements. If true,

$_{508}$ this would lead to overestimates of retrieved rain rate by ≈ 1 dB if the $\mu - D_m$ relationship of

$_{509}$ Williams et al. (2014) is used, or 2 dB if an exponential distribution or the $\mu - \Lambda$ relationship

$_{510}$ of Cao et al. (2008) is used. We find that the μ retrieval exhibits sensitivity to the choice of

$_{511}$ drop oscillation model. A better understanding of raindrop oscillations would be useful to

$_{512}$ fully establish the accuracy of our retrieval technique.

$_{513}$ The variability in our radar retrieved μ could simply be natural variability of the DSD

$_{514}$ between convective and stratiform rainfall; there may not be a universal $\mu - D_0$ relationship.

$_{515}$ More case studies are desirable to investigate this further.

$_{516}$ The μ retrieval technique employed here offers improvements over the radar estimates

$_{517}$ of Illingworth and Caylor (1991) and Thurai et al. (2008). Illingworth and Caylor (1991)

$_{518}$ did not take into account the imperfect co-location of the H and V sample volumes on

$_{519}$ measurements of ρ_{hv}, the effect of drop oscillations, or the fact their ρ_{hv} estimates would

$_{520}$ be biased low by averaging short time-series. Each of these effects would cause μ to be

22

underestimated. The same is true of Thurai et al. (2008), however drop shapes measured by 2DVD measurements include oscillations, and so are included in their μ estimates.

The new error statistics of ρ_{hv} presented here could aid operational applications that require uncertainty on $\hat{\rho}_{hv}$ to be quantified, or use averages of $\hat{\rho_{hv}}$. The use of L operationally to retrieve μ is limited by use of rapid scan rates and the corresponding few independent I and Q samples. However, assuming that μ is a smoothly varying parameter, averaging L could help improve rain rate retrievals; the uncertainty on operationally retrieved rain rates using the retrieval technique presented here is estimated to be approximately $\pm 12.5\%$. Practically, retrieved rain rates are less affected by changes in higher values of μ compared to changes in lower values. Therefore, operationally, simply being able to distinguish regions of 'high' and 'low' μ with L could be sufficient to provide an improvement over existing $Z - Z_{DR}$ retrieval techniques.

APPENDIX

The effect of imperfectly co-located H and V samples on ρ_{hv}

Consider two measurements of the (complex) amplitudes at horizontal and vertical polarisation A_H and A_V. If the two polarisations do not have perfectly matched sample volumes, then each amplitude is the sum of (i) a component which is common to both polarisations C_H, C_V, (ii) a component which is different for each polarisation D_H, D_V:

$$A_H = C_H + D_H \tag{A1}$$

(and similarly $A_V = C_V + D_V$). The co-polar correlation coefficient is:

$$\rho_{hv} = \frac{\sum A_H A_V^*}{\sqrt{\sum |A_H|^2 \sum |A_V|^2}} \tag{A2}$$

where the sums $\sum$ are taken over many reshufflings of the raindrops. Substituting in the expressions for A_H and A_V leads to:

$$\rho_{hv} = \frac{\sum C_H C_V^* + \sum D_H C_V^* + \sum C_H D_V^* + \sum D_H D_V^*}{\sqrt{\sum |C_H + D_H|^2 \sum |C_V + D_V|^2}} \quad \text{(A3)}$$

542 The first term in the numerator dominates as the number of pulses is increased. This is

543 because D_H, D_V, are uncorrelated ith C_V, C_H (because the reshuffling of particles in the

544 different sample volumes is not connected or organised in any way), while C_H and C_V are

545 highly correlated (because the true ρ_{hv} is close to 1). The final term is small because D_H,

546 D_V, are not correlated (by the same argument), and this term is small in any case since

547 $|D| \ll |C|$)

548   This leaves us with:

$$\rho_{hv} = \frac{\sum C_H C_V^*}{\sqrt{\sum |C_H + D_H|^2 \sum |C_V + D_V|^2}} \quad \text{(A4)}$$

549 In the case of a perfect radar with perfect co-location of the H and V samples, then D_H, D_V

550 are zero and we get a correlation coefficient which is the true ρ_{hv} which we are trying to

551 obtain (ie setting $A = C$ in equation A2).

552   In general, for an imperfect radar, we have $D_H, D_V > 0$ and from the results above we

553 see that:

$$\rho_{hv} = \rho_{hv}^{\text{true}} \times f_{hv}^{max} \quad \text{(A5)}$$

554 where

$$f_{hv}^{max} = \left(\frac{\sum |C_H|^2}{\sum |C_H + D_H|^2} \times \frac{\sum |C_V|^2}{\sum |C_V + D_V|^2} \right)^{1/2} \quad \text{(A6)}$$

555 This result is directly analogous to the results of Bringi et al. (1983) on ρ_{hv} in the presence

556 of noise. If we identify C as our "signal" and D as our "noise" this equation is identical to

557 Equation A1.

558   Crucially, the relationship between the true ρ_{hv} (ρ_{hv}^{true}) and the one which is actually

559 observed is determined simply by how much power (on average over many pulses) comes

24

from the particles which are different for the H and V sample volumes, relative to how much power comes from the particles which are common to the H and V sample volumes, and that this factor should be constant for different microphysical situations. Thus if we can measure ρ_{hv} in drizzle where we know $\rho_{hv}^{\text{true}} = 1$, then the measured ρ_{hv} is simply equal to f_{hv}^{max}. This scaling factor can then be applied to data from all other situations.

Acknowledgements

REFERENCES

Andrić, J., M. R. Kumjian, D. S. Zrnić, J. M. Straka, and V. M. Melnikov, 2013: Polarimetric signatures above the melting layer in winter storms: An observational and modeling study. *Journal of Applied Meteorology and Climatology*, **52 (3)**, 682–700.

Balakrishnan, N., and D. Zrnic, 1990: Use of polarization to characterize precipitation and discriminate large hail. *Journal of the atmospheric sciences*, **47 (13)**, 1525–1540.

Beard, K. V., V. Bringi, and M. Thurai, 2010: A new understanding of raindrop shape. *Atmospheric Research*, **97 (4)**, 396–415.

Beard, K. V., and R. J. Kubesh, 1991: Laboratory measurements of small raindrop distortion. Part 2: Oscillation frequencies and modes. *Journal of the atmospheric sciences*, **48 (20)**, 2245–2264.

Brandes, E. A., and K. Ikeda, 2004: Freezing-level estimation with polarimetric radar. *Journal of Applied Meteorology*, **43 (11)**, 1541–1553.

Brandes, E. A., G. Zhang, and J. Vivekanandan, 2002: Experiments in rainfall estimation with a polarimetric radar in a subtropical environment. *Journal of Applied Meteorology*, **41 (6)**, 674–685.

Bringi, V. N., and V. Chandrasekar, 2001: *Polarimetric Doppler Weather Radar, Principles and Applications*. Cambridge University Press, Cambridge, UK.

Bringi, V. N., T. A. Seliga, and S. M. Cherry, 1983: Statistical properties of the dual-polarization differential reflectivity (Z_{DR}) radar signal. *IEEE Trans. Geosci. Rem Sens.*, **GE-21 (2)**, 215 –220, doi:10.1109/TGRS.1983.350491.

26

Cao, Q., and G. Zhang, 2009: Errors in estimating raindrop size distribution parameters employing disdrometer and simulated raindrop spectra. *Journal of Applied Meteorology and Climatology*, **48 (2)**, 406–425.

Cao, Q., G. Zhang, E. Brandes, T. Schuur, A. Ryzhkov, and K. Ikeda, 2008: Analysis of video disdrometer and polarimetric radar data to characterize rain microphysics in Oklahoma. *Journal of Applied Meteorology and Climatology*, **47 (8)**, 2238–2255.

Caylor, I. J., 1989: Radar observations of maritime clouds using dual linear polarisation. Ph.D. thesis, University of Manchester, Manchester, UK.

Caylor, J., and A. J. Illingworth, 1989: Identification of the bright band and hydrometeors using co-polar dual polarization radar. *Preprints, 24th Conf. on Radar Meteorology, Florida, USA, Amer. Meteor. Soc*, 352–357.

Doviak, R. J., and Zrnic, 2006: *Doppler Radar and Weather Observations*. Dover Publications, Inc., Mineola, New York, USA.

Fisher, R. A., 1915: Frequency distribution of the values of the correlation coefficient in samples from an indefinitely large population. *Biometrika*, **10 (4)**, 507–521.

Giangrande, S. E., J. M. Krause, and A. V. Ryzhkov, 2008: Automatic designation of the melting layer with a polarimetric prototype of the WSR-88D radar. *Journal of Applied Meteorology and Climatology*, **47 (5)**, 1354–1364.

Goddard, J., J. D. Eastment, and M. Thurai, 1994: The chilbolton advanced meteorological radar: A tool for multidisciplinary atmospheric research. *Electronics & communication engineering journal*, **6 (2)**, 77–86.

Illingworth, A. J., and I. J. Caylor, 1991: Co-polar correlation measurements of precipitation. *Preprints, 25th Int. Conf. on Radar Meteorology, Paris, France, Amer. Meteor. Soc*, 650–653.

Jameson, A., 1987: Relations among linear and circulur polarization parameters measured in canted hydrometeors. *Journal of Atmospheric and Oceanic Technology*, **4 (4)**, 634–646.

Jameson, A., and A. Kostinski, 1998: Fluctuation properties of precipitation. Part ii: Reconsideration of the meaning and measurement of raindrop size distributions. *Journal of the atmospheric sciences*, **55 (2)**, 283–294.

Johnson, R. W., D. V. Kliche, and P. L. Smith, 2014: Maximum likelihood estimation of gamma parameters for coarsely binned and truncated raindrop size data. *Quarterly Journal of the Royal Meteorological Society*, **140 (681)**, 1245–1256.

Liu, L., V. N. Bringi, V. Chandrasekar, E. A. Mueller, and A. Mudukutore, 1994: Analysis of the co-polar correlation coefficient between horizontal and vertical polarizations. *Journal of Atmospheric and Oceanic Technology*, **11 (4)**, 950–963.

McFarquhar, G. M., 2004: The effect of raindrop clustering on collision-induced break-up of raindrops. *Quarterly Journal of the Royal Meteorological Society*, **130 (601)**, 2169–2190.

Papoulis, A., 1965: Probability, random variables, and stochastic processes.

Park, H. S., A. V. Ryzhkov, D. Zrnic, and K.-E. Kim, 2009: The hydrometeor classification algorithm for the polarimetric WSR-88D: Description and application to an mcs. *Weather and Forecasting*, **24 (3)**, 730–748.

Rogers, R., 1989: Raindrop collision rates. *Journal of the Atmospheric Sciences*, **46 (15)**, 2469–2472.

Sachidananda, M., and D. Zrnic, 1989: Efficient processing of alternately polarized radar signals. *Journal of Atmospheric and Oceanic Technology*, **6 (1)**, 173–181.

Schafer, R., S. Avery, P. May, D. Rajopadhyaya, and C. Williams, 2002: Estimation of rainfall drop size distributions from dual-frequency wind profiler spectra using deconvolu-

639 tion and a nonlinear least squares fitting technique. *Journal of Atmospheric and Oceanic*
640 *Technology*, **19 (6)**, 864–874.

641 Seliga, T., and V. Bringi, 1976: Potential use of radar differential reflectivity measurements
642 at orthogonal polarizations for measuring precipitation. *Journal of Applied Meteorology*,
643 **15 (1)**, 69–76.

644 Szakáll, M., K. Diehl, S. K. Mitra, and S. Borrmann, 2008: A wind tunnel study on the
645 oscillation of freely falling raindrops. *Proc. Fifth European Conf. on Radar in Meteorology*
646 *and Hydrology (ERAD 2008)*.

647 Szakáll, M., S. Kessler, K. Diehl, S. K. Mitra, and S. Borrmann, 2014: A wind tunnel study
648 of the effects of collision processes on the shape and oscillation for moderate-size raindrops.
649 *Atmospheric Research*, **142**, 67–78.

650 Szakáll, M., S. K. Mitra, K. Diehl, and S. Borrmann, 2010: Shapes and oscillations of falling
651 raindrops — a review. *Atmospheric Research*, **97 (4)**, 416–425.

652 Tabary, P., A. Le Henaff, G. Vulpiani, J. Parent-du Châtelet, and J. Gourley, 2006: Melting
653 layer characterization and identification with a C-band dual-polarization radar: A long-
654 term analysis. *Proc. Fourth European Radar Conf*, 17–20.

655 Tang, L., J. Zhang, C. Langston, J. Krause, K. Howard, and V. Lakshmanan, 2014: A
656 physically based precipitation–nonprecipitation radar echo classifier using polarimetric
657 and environmental data in a real-time national system. *Weather and Forecasting*, **29 (5)**,
658 1106–1119.

659 Thurai, M., and V. Bringi, 2005: Drop axis ratios from a 2D video disdrometer. *Journal of*
660 *Atmospheric & Oceanic Technology*, **22 (7)**.

661 Thurai, M., D. Hudak, and V. Bringi, 2008: On the possible use of co-polar correlation coeffi-

cient for improving the drop size distribution estimates at C band. *Journal of Atmospheric and Oceanic Technology*, **25 (10)**, 1873–1880.

Thurai, M., M. Szakáll, V. N. Bringi, and S. K. Mitra, 2013: Collision-induced drop oscillations from wind-tunnel experiments. *Proc. 36th Conference on Radar Meteorology.*

Tokay, A., A. Kruger, and W. F. Krajewski, 2001: Comparison of drop size distribution measurements by impact and optical disdrometers. *Journal of Applied Meteorology*, **40 (11)**, 2083–2097.

Torlaschi, E., and Y. Gingras, 2003: Standard deviation of the co-polar correlation coefficient for simultaneous transmission and reception of vertical and horizontal polarized weather radar signals. *Journal of Atmospheric and Oceanic Technology*, **20 (5)**, 760–766.

Ulbrich, C. W., 1983: Natural variations in the analytical form of the raindrop size distribution. *Journal of Climate and Applied Meteorology*, **22 (10)**, 1764–1775.

Unal, C., 2015: High resolution raindrop size distribution retrieval based on the doppler spectrum in the case of slant profiling radar. *Journal of Atmospheric and Oceanic Technology*, **(2015)**.

Williams, C. R., 2002: Simultaneous ambient air motion and raindrop size distributions retrieved from UHF vertical incident profiler observations. *Radio Science*, **37 (2)**, 8–1.

Williams, C. R., and Coauthors, 2014: Describing the shape of raindrop size distributions using uncorrelated raindrop mass spectrum parameters. *Journal of Applied Meteorology and Climatology*, **53 (5)**, 1282–1296.

Wilson, D. R., A. J. Illingworth, and T. M. Blackman, 1997: Differential doppler velocity: A radar parameter for characterizing hydrometeor size distributions. *Journal of Applied Meteorology*, **36 (6)**, 649–663.

List of Tables

TABLE 1. Typical rain rates (R) for each of the case studies, calculated from disdrometer measurements (April) and radar retrieved N_0, D_0 and μ values (January, May and November)

Month	Typical R (mm hr^{-1})	Peak R (mm hr^{-1})
31 January 2014	1−3	8
25 April 2014	2−3	7
22 May 2014	2−7	>30
25 November 2014	2−5	10

List of Figures

5   (a) A comparison of the confidence intervals calculated using the new method and that of Torlaschi and Gingras (2003) in rain ($\overline{\rho_{hv}} = 0.98$) and (b) the bias introduced by averaging $\hat{\rho_{hv}}$ instead of $\hat{L}$, as a function of N_{IQ}. For all N_{IQ}, the lower confidence interval is higher for the Torlaschi and Gingras (2003) method, particularly for lower N_{IQ}, due to the asymmetric nature of the confidence intervals on ρ_{hv} using the new method. Averaging $\hat{\rho_{hv}}$ and not $\hat{L}$ for small N_{IQ} can lead to a large bias.   40

6   (a) Comparison of mean drop axis ratios as a function of equivalent drop diameter (D) from recent experiments of Thurai and Bringi (2005), Szakáll et al. (2008) and the 4$^{\text{th}}$ order polynomial fit of older experimental data constructed by Brandes et al. (2002). The model of Thurai and Bringi (2005) has been adapted so that drops are spherical for $D < 1$ mm. Panels (b)—(d) show radar and disdrometer Z_{DR} comparisons calculated using Thurai and Bringi (2005), Szakáll et al. (2008) and Brandes et al. (2002) from a 5 hour dwell over a nearby Joss-Waldvogel RD-80 impact disdrometer (approximately 7 km away) in a frontal rain band on 25 April 2014. The time resolution of the radar measurements was decreased to 30 s to match the integration time of the disdrometer. At a 1.5° elevation angle, the radar was sampling rain at a height of ≈ 183 m above the disdrometer. The dashed line is a 1:1 line. The smallest biases are achieved with the Thurai and Bringi (2005) model, especially for smaller Z_{DR}, suggesting that these shapes best represent those of natural rain drops. Therefore, this model is chosen for the analysis.   41

7   Predicted L and Z_{DR} values for gamma distributions of $\mu = $ -1 (solid) and 16 (dashed) with no oscillations (grey), and including oscillations (black). The inclusion of drop oscillations are crucial to interpretation of L and Z_{DR} measurements. The f_{hv}^{max} is assumed to be 0.9963 to match the case study in Section 7.   42

8   Theoretical L and Z_{DR} computed using Gans theory for gamma distributions with μ = -1, 0, 2, 4, 8, 12 and 16, using Thurai and Bringi (2005) mean drop axis ratios and oscillation model described in Section 6b. The precision of L required to estimate μ decreases as Z_{DR} increases. The f_{hv}^{max} is assumed to be 0.9963 to match the case study in Section 7.   43

9   (a) 2D PDF of L and Z_{DR} observations, and (b) normalised 2D PDF such that the distribution equals 1 for each Z_{DR} bin for observations of L and Z_{DR} collected from dwells on 25 November 2014. L is binned ever 0.02, and Z_{DR} every 0.05 dB. Overplotted are theoretical L and Z_{DR} computed using Gans theory for gamma distributions of μ = -1, 0, 2, 4, 8, 12 and 16. Typical errors on L and Z_{DR} are shown as error bars; the error on Z_{DR} is very small. The grey dashed line is the predicted L and Z_{DR} observations using DSD parameters from the power-law fit to disdrometer measurements in Williams et al. (2014). The black dashed line is the predicted L and Z_{DR} observations using the $\mu - \Lambda$ relationship of Cao et al. (2008). The f_{hv}^{max} for this day is measured to be 0.9963.   44

10   Box plot of retrieved μ as a function of Z_{DR} for Z_{DR} bins of 0.2 dB on 25 November 2014, showing the median and inter-quartile range of the data.   45

11   Median retrieved μ as a function of Z_{DR} for Z_{DR} bins of 0.1 dB for case studies of 31 January, 25 April, 22 May and 25 November 2014. The solid line is the predicted μ as a function of Z_{DR} from the power law fit to disdrometer measurements of Williams et al. (2014), and σ_μ corresponds to the upper and lower bounds that contain 55% of the data. The solid black line shows the predicted $\mu - Z_{DR}$ using the $\mu - \Lambda$ relationship of Cao et al. (2008).   46
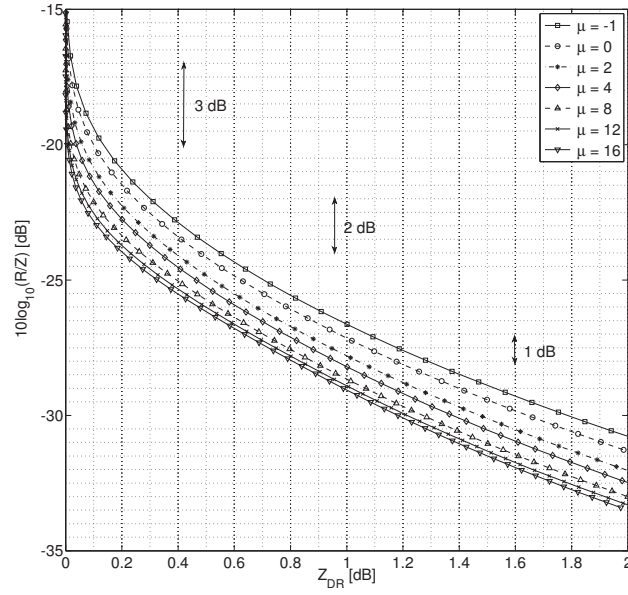
FIG. 1. Rain rate (in dB referenced to 1 mm hr^{-1}) per unit radar reflectivity as a function of Z_{DR} computed using Gans theory for gamma distributions of μ = -1, 0, 2, 4, 8, 12 and 16. The rain rate can vary by as much as 2.5 dB for a given pair of Z and Z_{DR} observations as a result of drop spectrum shape variability.
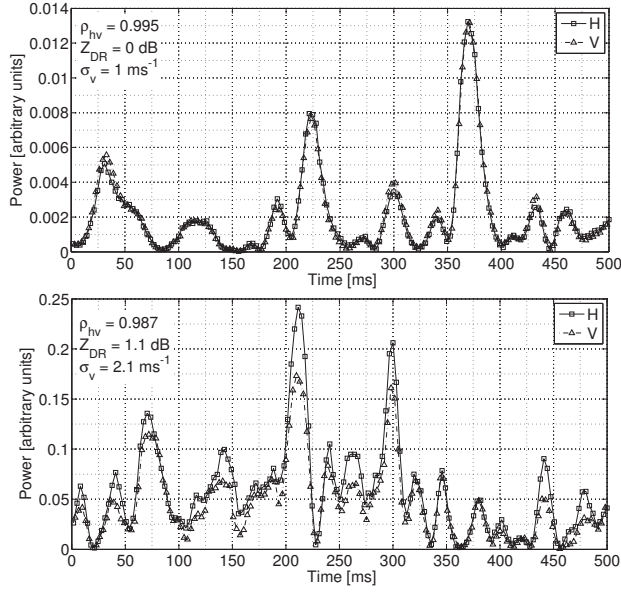
FIG. 2. Example time-series (0.5 s) for single 75 m gates from 1.5° elevation dwells in (*a*) drizzle ($Z_{DR} = 0$ dB) at 1203 UTC on 6 February 2014, and (*b*) heavier rainfall ($Z_{DR} = 1.1$ dB) at 1706 UTC on 31 January 2014. For both examples, SNR > 40 dB. For drizzle, the H and V echo time-series vary in unison as the drops are all spherical. In heavier rainfall, the broader axis ratio distribution causes the H and V time-series to be less correlated. The rate of fluctuation of the signals is determined by the Doppler spectral width.

FIG. 3. The frequency distribution of (a) $\hat{\rho_{hv}}$ calculated from 1159 time-series (0.21 s, 75 m gates) in drizzle ($Z_{DR} < 0.1$ dB) and (b) $\hat{L} = -\log_{10}(1-\hat{\rho_{hv}})$. The data was collected at 1203 UTC on 6 February 2014 during a 1.5° elevation dwell and has very high SNR (> 40 dB). σ_v for these data ranges between 0.9—1.3 ms^{-1}. Overplotted on $\hat{L}$ is a Gaussian curve with same mean and standard deviation as the measured distribution.
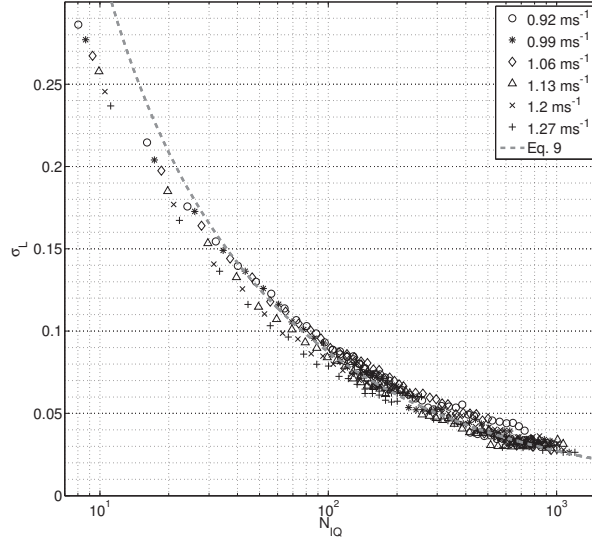
FIG. 4. σ_L as a function of the number of independent I and Q samples used to estimate L for high SNR measurements in drizzle ($Z_{DR} < 0.1$ dB, SNR > 40 dB) at 1203 UTC on 6 February. Different markers correspond to different Doppler spectral widths.

FIG. 5. (a) A comparison of the confidence intervals calculated using the new method and that of Torlaschi and Gingras (2003) in rain ($\overline{\rho_{hv}} = 0.98$) and (b) the bias introduced by averaging $\hat{\rho_{hv}}$ instead of $\hat{L}$, as a function of N_{IQ}. For all N_{IQ}, the lower confidence interval is higher for the Torlaschi and Gingras (2003) method, particularly for lower N_{IQ}, due to the asymmetric nature of the confidence intervals on ρ_{hv} using the new method. Averaging $\hat{\rho_{hv}}$ and not $\hat{L}$ for small N_{IQ} can lead to a large bias.

FIG. 6. (a) Comparison of mean drop axis ratios as a function of equivalent drop diameter (D) from recent experiments of Thurai and Bringi (2005), Szakáll et al. (2008) and the 4$^{\text{th}}$ order polynomial fit of older experimental data constructed by Brandes et al. (2002). The model of Thurai and Bringi (2005) has been adapted so that drops are spherical for $D < 1$ mm. Panels (b)—(d) show radar and disdrometer Z_{DR} comparisons calculated using Thurai and Bringi (2005), Szakáll et al. (2008) and Brandes et al. (2002) from a 5 hour dwell over a nearby Joss-Waldvogel RD-80 impact disdrometer (approximately 7 km away) in a frontal rain band on 25 April 2014. The time resolution of the radar measurements was decreased to 30 s to match the integration time of the disdrometer. At a 1.5° elevation angle, the radar was sampling rain at a height of ≈ 183 m above the disdrometer. The dashed line is a 1:1 line. The smallest biases are achieved with the Thurai and Bringi (2005) model, especially for smaller Z_{DR}, suggesting that these shapes best represent those of natural rain drops. Therefore, this model is chosen for the analysis.
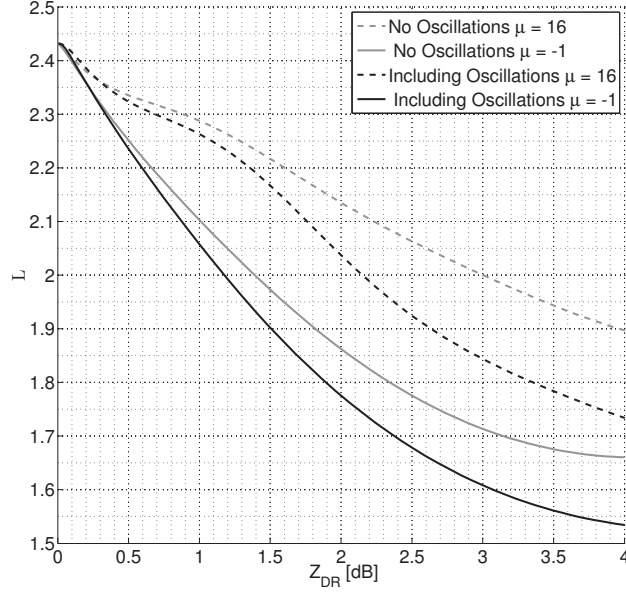
FIG. 7. Predicted L and Z_{DR} values for gamma distributions of $\mu = $ -1 (solid) and 16 (dashed) with no oscillations (grey), and including oscillations (black). The inclusion of drop oscillations are crucial to interpretation of L and Z_{DR} measurements. The f_{hv}^{max} is assumed to be 0.9963 to match the case study in Section 7.
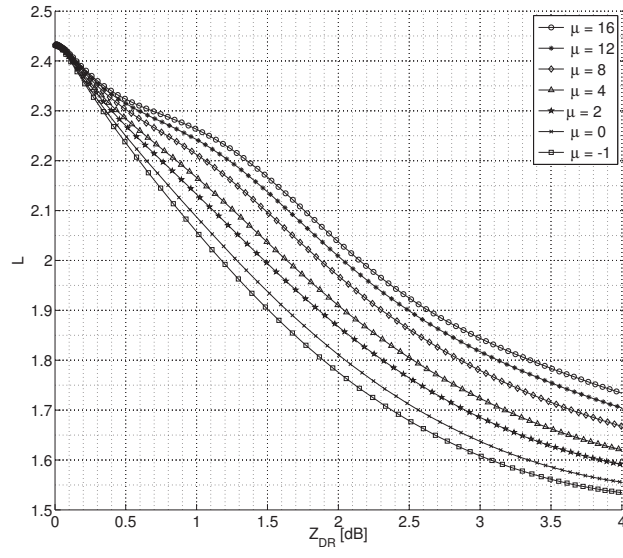
FIG. 8. Theoretical L and Z_{DR} computed using Gans theory for gamma distributions with μ = -1, 0, 2, 4, 8, 12 and 16, using Thurai and Bringi (2005) mean drop axis ratios and oscillation model described in Section 6b. The precision of L required to estimate μ decreases as Z_{DR} increases. The f_{hv}^{max} is assumed to be 0.9963 to match the case study in Section 7.
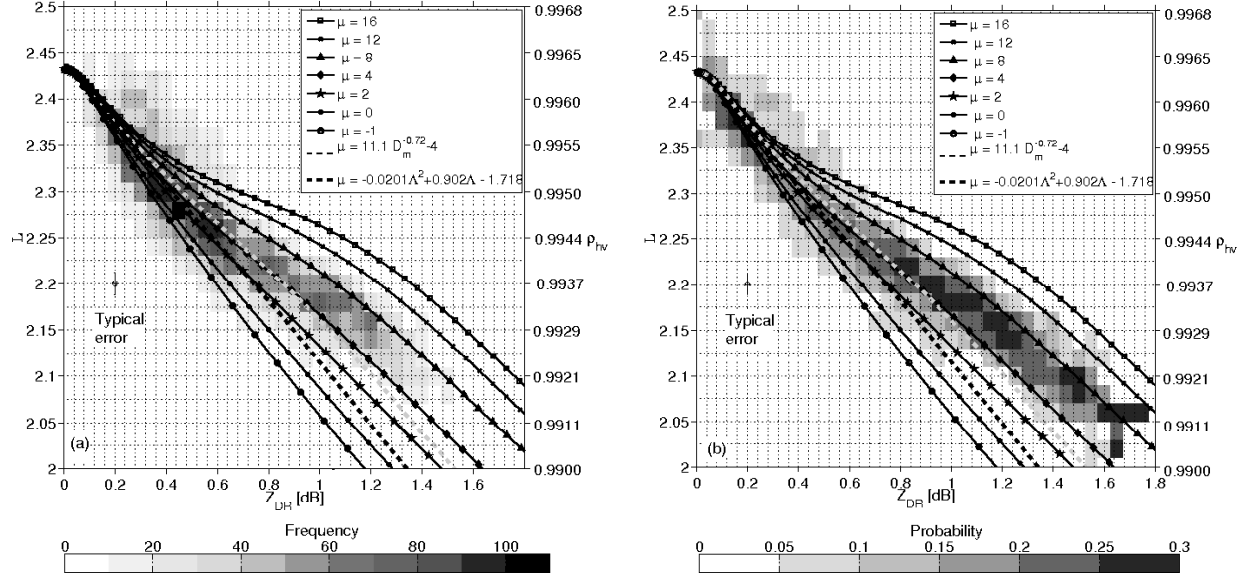
Fig. 9. (a) 2D PDF of L and Z_{DR} observations, and (b) normalised 2D PDF such that the distribution equals 1 for each Z_{DR} bin for observations of L and Z_{DR} collected from dwells on 25 November 2014. L is binned ever 0.02, and Z_{DR} every 0.05 dB. Overplotted are theoretical L and Z_{DR} computed using Gans theory for gamma distributions of $\mu = -1$, 0, 2, 4, 8, 12 and 16. Typical errors on L and Z_{DR} are shown as error bars; the error on Z_{DR} is very small. The grey dashed line is the predicted L and Z_{DR} observations using DSD parameters from the power-law fit to disdrometer measurements in Williams et al. (2014). The black dashed line is the predicted L and Z_{DR} observations using the $\mu - \Lambda$ relationship of Cao et al. (2008). The f_{hv}^{max} for this day is measured to be 0.9963.
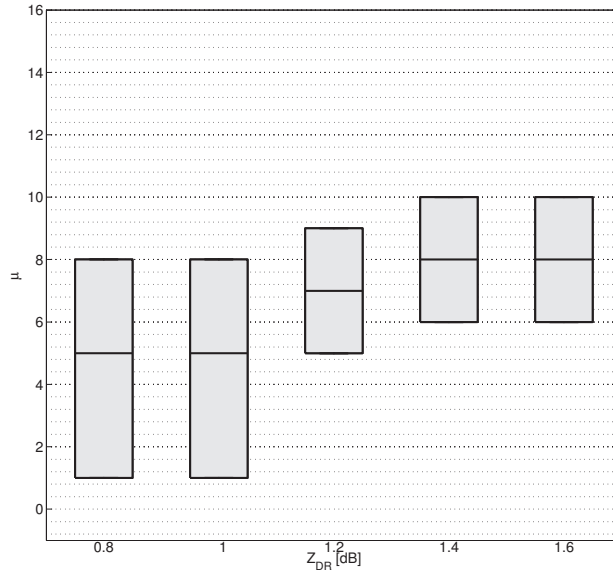
FIG. 10. Box plot of retrieved μ as a function of Z_{DR} for Z_{DR} bins of 0.2 dB on 25 November 2014, showing the median and inter-quartile range of the data.
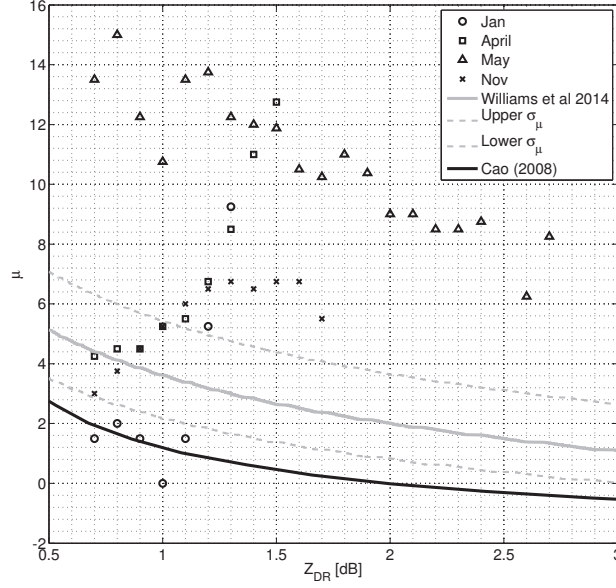
FIG. 11. Median retrieved μ as a function of Z_{DR} for Z_{DR} bins of 0.1 dB for case studies of 31 January, 25 April, 22 May and 25 November 2014. The solid line is the predicted μ as a function of Z_{DR} from the power law fit to disdrometer measurements of Williams et al. (2014), and σ_μ corresponds to the upper and lower bounds that contain 55% of the data. The solid black line shows the predicted $\mu - Z_{DR}$ using the $\mu - \Lambda$ relationship of Cao et al. (2008).